# Impact of Surface Wettability on Dynamics of Supercooled Water Confined in Nitrogen-Doped Ordered Mesoporous Carbon



| | |
|---|---|
| Journal: | *Physical Chemistry Chemical Physics* |
| Manuscript ID | CP-ART-09-2018-005670.R1 |
| Article Type: | Paper |
| Date Submitted by the Author: | 02-Oct-2018 |
| Complete List of Authors: | Wiener, Clinton; University of Akron, Department of Polymer Engineering<br>Qiang, Zhe; The University of Akron, Department of Polymer Engineering<br>Xia, Yanfeng; The University of Akron, Department of Polymer Engineering<br>Tyagi, Madhusudan; NIST, NIST Center for Neutron Research<br>Vogt, Bryan; University of Akron, Polymer Engineering |
| | |

Journal Name

ARTICLE

# Impact of Surface Wettability on Dynamics of Supercooled Water Confined in Nitrogen-Doped Ordered Mesoporous Carbon

Received 00th January 20xx,
Accepted 00th January 20xx

DOI: 10.1039/x0xx00000x

www.rsc.org/

*Clinton G. Wiener,*[a, ‡, †] *Zhe Qiang,*[a, ‡, †] *Yanfeng Xia,*[b] *Madhusudan Tyagi,*[c] *and Bryan D. Vogt*[a, *]

Confinement of water to nanoscale dimensions enables substantial supercooling through disruption of the hydrogen bonding network. However, there remain questions associated with the relative importance of the nature of the water-surface interactions relative to physical confinement defined by the pore geometry on the dynamics of supercooled water. Here, a simple route to tune the surface wetting properties through nitrogen doping of carbon is reported. This method leads to nearly indistinguishable mesopore sizes to enable separation of surface wettability and pore size effects. Quasielastic neutron scattering (QENS) is used to probe the proton dynamics of water confined within the mesopores with an average diameter of 4.85 ± 0.05 nm as a function of temperature from 267K to 189K. The motions of water in the mesopores follow jump-diffusion. For the temperatures examined, the diffusivity of water in the mesopores decreases with increasing nitrogen doping of the carbon framework. The activation energy associated with proton dynamics increases by approximately 30% with N-doping when compared to undoped carbon surface, which is attributed to the enhanced surface wettability (favorable interactions between water and pore surface). This acts to provide an energy barrier for the water motions. This work suggests that the influence of surface chemistry on the dynamics of supercooled water confined in mesopores is less than the influence of nanopore size.

## Introduction

Volumetric expansion associated with water crystallization (ice) is extremely detrimental to infrastructure and buildings,[1] while icing on surfaces decreases the efficiency of wind turbines[2] and poses a major safety risk for many industries. Due to these industrial drivers, there have been significant efforts[3, 4,4] in developing routes to prevent or control ice formation. One common route to suppress water crystallization is confining water molecules at the nanoscale between hard surfaces where the liquid-solid surface interactions perturb the hydrogen bonding structure of water.[5] Understanding how these surface interactions impact the structure and thermodynamics of water is of fundamental interest for many fields from catalysis to biology to food preservation technologies.[6-8] A majority of the prior work on this topic has focused exclusively on the geometric constraints (dimension and shape of the pores) where the length scale of the minor dimension of pores is the dominant factor for inhibiting water crystallization for a constant wall chemistry.[6, 9, 10] For example with carbon nanotubes, there is a maximum in the freezing depression at a tube diameter of 1.1 nm,[11] but the phase of the ice formed can also be impacted by the confinement.[12] The suppression of ice crystallization in these nanopores allows insight into amorphous water behavior at temperatures inaccessible in the bulk on cooling due to the rapid homogeneous nucleation of ice through examination of their dynamics.[13, 14] However, the crystallization temperature for water in porous carbon has been reported to be lower than that for water in silica with similar pore geometries.[15, 16] This leads to questions about how the interactions of water with the pore wall will impact the measured dynamics of water in nanopores.

Systematic investigations of the influence of the hydrophobicity of the pore surface have been challenged by the ability to maintain the pore size, while developing a homogeneous surface chemistry that is systematically varied. Typical modification involves the chemical grafting of pendant functional groups to the pore walls.[17] For example, methylation of hydrophilic silica (MCM-41) by a silane coupling agent leads to increased water mobility in the mesopores at supercooled temperatures,[18] but this treatment leads to a finite change in thickness as well as change in functionality with the loss of hydrogen bonding of the water with the

[a] *Department of Polymer Engineering, University of Akron, Akron, OH, 44325, USA*
[b] *Department of Polymer Science, University of Akron, Akron, OH, 44325, USA*
[c] *Center for Neutron Research, National Institute of Standards and Technology, Gaithersburg, MD, 20899, USA and Department of Materials Science and Engineering, University of Maryland, College Park, MD 20742 USA*
† Present address: 3M, Center St., St. Paul, MN, 55144 (C.G.W.)
Department of Chemical and Biological Engineering, Northwestern University, Evanston, IL, USA, 60208 (ZQ)
‡*These authors contributed equally.*

Electronic Supplementary Information (ESI) available: Adsorption-desorption isotherms and TEM images of all OMC samples, MSD results for cooling rate of 0.8K/min from room temperature to 4K and then reheating at 2K/min for all OMC samples and elastic incoherent structure factor (EISF) calculated from Lorentzian fits of full energy window scans are included. See DOI: 10.1039/x0xx00000x

surface silanols after treatment. These effects inhibit clear understanding of how wettability impacts water dynamics in confinement.[19] Moreover, this pore modification could lead to roughness and heterogeneity in the pore channel due to incomplete functionalization, where the packing efficacy of the silane agent determines the gaps present.[20]

In contrast to the large variation in the surface chemistry from methylation of silica, beginning with a carbon framework and incorporating nitrogen heteroatoms into the framework leads to a gradual change in the relative hydrophilicity that can be readily tuned.[21] Small changes in the nitrogen content significantly change the surface energy of carbon[22] and associated hydrophobicity of nanoporous materials.[23] In this work, a series of ordered mesoporous carbons with nitrogen content from 0 to 4.1 at % with almost identical pore size (± 0.05 nm), porosity (± 0.04 $cm^3$ $g^{-1}$), and surface area ( ± 30 $m^2$ $g^{-1}$) were synthesized using a soft-templating method.[24] The water contact angle of water changes from approximately 90° for the undoped carbon to a wetted surface with a contact angle < 5° with 4.1 at % nitrogen in the carbon framework. Quasielastic neutron scattering (QENS) is used to probe the dynamics of water confined within the mesopores to provide insight into the impact of the framework chemistry on supercooled water confined in nanopores. With increasing nitrogen doping, the effective diffusivity of supercooled water within the mesopores decreases while the activation energy associated with water motions increases. These results illustrate how the chemistry of the confining surface impacts the dynamics of confined supercooled water.

## Experimental Section

### Materials

Pluronic® P123 ($M_w$ = 5,800 g/mol, $PEO_{20}$-$PPO_{70}$-$PEO_{20}$), sodium hydroxide (NaOH, >97%), ethanol (>99%), phenol (>99%), formaldehyde (ACS reagent, 37 wt% in $H_2O$, contains 10-15% methanol as stabilizer), hydrochloric acid (HCl, ACS reagent, 37%), and melamine (>99%) were all obtained from Sigma Aldrich and used as received. Low molecular-weight phenolic resin (resol) was synthesized from condensation of phenol and formaldehyde under basic conditions using NaOH following previously reported procedures.[25]

### Synthesis of the OMC and N-doped OMCs

To prepare the ordered mesoporous carbon (OMC), Pluronic P123 was dissolved under stirring at 600 rpm for 1 h at 45 °C in pre-synthesized resol (20 wt% in ethanol) at a molar ratio of phenol : P123 = 1:0.007 (mass ratio of resol : P123 = 1 :0.33). The ethanol in the solution was evaporated in a glass petri dish at room temperature for 12 h. The nominally dry resol-Pluronic P123 mixture was then heated at 100 °C for 24 h to crosslink the resol. The crosslinked products held in an alumina boat were calcined in a tube furnace (SentroTech Inc.) at 350°C for 2 h under $N_2$ protection to remove the Pluronic P123 and further crosslink the resol. For the synthesis of nitrogen-doped OMC (OMC-N), the mesoporous resol was then physically mixed with melamine using a MIRA grinder for 1 min at the desired mass ratio of melamine to mesoporous resol (0.02:1 and 0.05:1 for 1.9 % and 4.1% N doping, respectively). The mixture was then carbonized at 800°C using a temperature ramp of 5°C/min under $N_2$ protection with the temperature held at 800°C for 2 h. For the synthesis of OMC (no nitrogen doping), the crosslinked resol-Pluronic P123 mixture (without forming the mesoporous resol intermediate) was first heated to 600°C at 1°C/min, then to 800°C at 5°C/min with the temperature held at 800°C for 2 h.

### Characterization of OMC and N-doped OMCs

$N_2$ adsorption-desorption isotherms of OMC and OMC-N were measured using a TriStar II (Micromeritics) at 77K. From the adsorption isotherms, the specific surface area was determined by the Brunauer Emmett and Teller (BET) method[26] and the pore size distributions were determined by the Barrett, Joyner and Halenda (BJH)[27] model. The extent of doping was determined by X-ray photo-electron spectroscopy (XPS PHI5000 Versa Probe II Scanning XPS Microprobe, ULVAC-PHI, Inc.) using energies from 700 eV to 0 eV with a pass energy of 11.75 eV. The takeoff angle was 45°.

### Sample preparation via hydration

The carbon samples were first dried under vacuum at 100 °C overnight. The dried powder was placed in the top of a desiccator where the bottom was filled with DI water. The carbons were hydrated by condensation of water vapor with the mesopores in the closed desiccator, following procedures reported previously.[16, 28, 29] The level of hydration was determined from the mass change of the powder through controlling the exposure time (or by subsequent exposure to ambient to slightly decrease the water loading). To maintain the water content, the hydrated samples were sealed either in a crimped aluminum foil pouch for QENS measurements or crimped DSC pan. The samples sealed within their containers were allowed to equilibrate for 12 h prior to any measurements.

### DSC characterization

For QENS measurements, the non-frozen water (NFW) is only desired to ease analysis as crystallizable water will be convoluted with NFW. The crystallizable water will contribute to the instrument signal both above the freezing point as this is free water, and below as it forms ice with low mobility. To determine the maximum water loading for 100 % NFW, the hydration was incrementally decreased from full hydration (equilibrium) to 10 % water mass/ dry OMC mass.

### Characterization of water dynamics with QENS

For the water dynamics measurements, the mesoporous carbons were loaded with approximately 10 wt% water as this loading ensures 100 % NFW irrespective of the nitrogen doping to enable direct comparisons and determine the effect of

nitrogen doping on the water dynamics. QENS was used to elucidate the average molecular motions of water confined in the mesoporous of the OMC samples on cooling. QENS measurements were performed on the High Flux Backscattering Spectrometer (HFBS) at the NIST Center for Neutron Research (NCNR) with an energy window of 17 μeV and energy resolution of ± 0.85 μeV (HWHM) that corresponds to 0.14 ns < $\tau$< 3.8 ns with the Q range of 0.25Å$^{-1}$ to 1.75Å$^{-1}$.[30] Two measurement modes were used on the HFBS. The first was fixed window scan (FWS), where the hydrated samples were cooled at 0.8 K/min from room temperature to 4K and then re-heated at 0.8 K/min to room temperature. The mean square displacement (MSD) of the system was obtained from the FWS with the signal dominated by the protons in the adsorbed water. An estimate for the relative change in the proton dynamics on cooling and heating was obtained from the MSD. The second measurement mode was the full energy window mode with 6-8 h measurements at each temperature to obtain reasonable statistics to discern the motions in the sample. The full energy window data were fit using a delta function, a Lorentzian function, and a flat background. These functions were convoluted with instrument resolution as determined using a vanadium standard. In this representation, the convoluted delta function accounts for processes slower than could be resolved by the instrument. The Lorentzian function accounts for the average dynamic motion of water that is resolvable by the instrument larger than the minimum resolution and below the maximum window width. The flat background was used to account for very fast motions that were not captured by the instrument energy window. A single Lorentzian function could obtain good fits of the full energy window data with no trend in the residual error, which suggests that there is only one population of water resolvable by these measurements for the samples examined herein.

## Results and Discussion

The nitrogen doped ordered mesoporous carbons were synthesized by soft-templating through an ordered mesoporous phenolic polymer intermediate[25] and filling the mesopores with melamine during carbonization to provide a large N source for the dynamic integration of nitrogen heteroatoms into the framework. The doping content was controlled by the ratio of the mesoporous intermediate to melamine.[31] Figure 1A illustrates the XPS spectra, which demonstrate 1.9 at% and 4.1 at% nitrogen in the framework at mass ratio of mesoporous silica-phenolic polymer to melamine of 1:0.05 and 1:0.1, respectively. The nitrogen is predominately incorporated as pyrrolic and pyridinic functionalities in the carbon,[24] the later is known to hydrogen bond with water to increase the hydrophilicity of a carbon matrix.[32] The water contact angle decreases from nearly 90˚ (OMC-0N) to less than 20˚ (OMC-1.9N) to approximately 0˚ (OMC-4.1N) where xN represents the at % of N in OMC. Due to the low heteroatom content (<5 at%), most of water molecules within the N-doped ordered mesoporous carbon are still 'free' rather than hydrogen bonded with the pore surfaces, so the wettability of the pore walls should be the dominant effect of these chemistry differences on the supercooled water dynamics as will be discussed.

The adsorption-desorption isotherms of these mesoporous carbons exhibit a typical type IV behavior with a type H1 hysteresis, consistent with uniform cylindrical mesopores (Figure S1). This morphology is confirmed by TEM as shown in Figure S2. As shown in Figure 1B, the pore size distribution is nearly unchanged by the nitrogen doping at the levels examined. The average pore size decreases from 4.9 nm (ordered mesoporous carbon, OMC) to 4.8 nm (OMC-1.9N and OMC-4.1N, where the xN represents the at % of N in the OMC). We attribute the slight shift in the pore size to expansion of carbon framework from inclusion of heteroatoms.[24] Based on the work of Liu et al. for nanoporous silica,[33] the dynamic properties of supercooled water should be minimally impacted by this 0.1 nm variation in pore size.

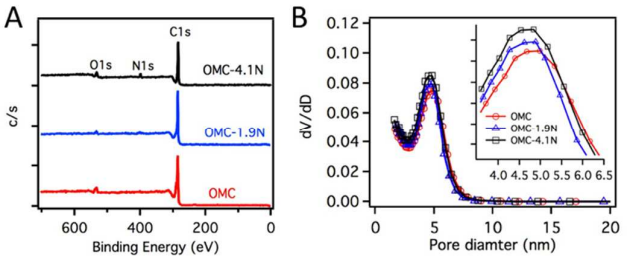


Figure 1. (A) XPS elemental analysis to determine the N content for the three OMCs used. (B) Pore size distribution determined from the N2 adsorption isotherms for the OMCs.

Figure 2 illustrates the DSC traces on cooling for the mesoporous carbons with water loadings greater than the maximum non-frozen water (NFW) fraction. As shown in Figure 2A, the OMC-0N containing 15 wt% water exhibits a large exotherm around 256K associated with the crystallization of water and several smaller exotherms associated with ice formation at lower temperatures with the lowest being approximately 240K. Assuming that the ice formed within these mesopores is hexagonal ice, $I_h$,[34] the enthalpy associated with these exotherms indicates that approximately 17% of the water froze as the sample was cooled to 200K. For the same water content (15 wt %) as shown in Figure 2B, the thermogram is significantly altered when the water is within the OMC-1.9N despite no significant change in the pore size distribution (Figure 1B). In this case, there is a broader exothermic peak centered around 233K, which suggests that the change in surface chemistry with only 1.9% N doping dramatically suppresses crystallization at this water loading. This differs from a recent report comparing water freezing in mesopores of silica and carbon frameworks, where the freezing and melting behavior were not impacted by the framework chemistry.[35] This difference may be associated with the exact chemistries examined and the water loading.

The multiple crystallization temperatures can be attributed to different environments for the water, either being

heterogeneities in the heteroatom distributions in the carbon framework or spatial dependencies based on location of the water molecules confined within the mesopores (e.g.,interfacial vs. bulk water).[36-39] The undoped OMC-0N contains residual oxygen molecules that could provide local hydrophilic patches on the carbon framework wall. Increasing the N doping increases the hydrophilicity to facilitate water loading within the mesopores, but at higher water loading for OMC-4.1N (19 wt %) the amount of NFW only modestly increases. This results in a sharp exothermic peak at approximately 238 K associated with an appreciable fraction of the water crystallizing. Interestingly, the depression in the crystallization temperature is slightly less than that of the OMC-1.9N, which suggests that the effect of the framework surface chemistry on the freezing point depression is dependent on the water loading in the mesopores as one might assume that the surface chemistry effect would scale directly with the hydrophilicity of the surface. These differences could be attributed to interfacial and bulk-like environments for water within the mesopores that depends on their proximity to the framework wall. The additional (weak) peaks in the DSC thermogram for the OMC-4.1N with increased water loading in comparison to the other compositions is also consistent with multiple environments for water within these mesopores. Through systematic modification of the water loading, the maximum NFW content for the OMC-0N, OMC-1.9N and OMC-4.1N was determined to be 12.4 wt %, 12.7wt% and 14.5 wt% water, respectively.

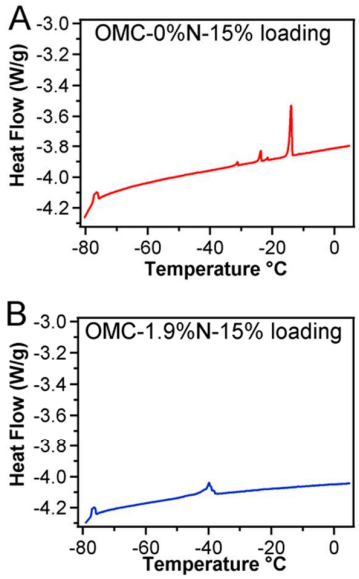


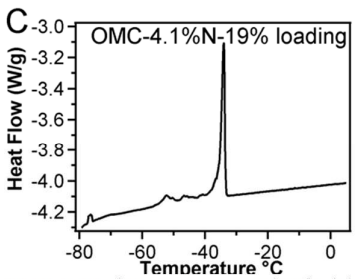


**Figure 2**. DSC thermograms on cooling for (A) OMC-0N containing 15 wt % water, (B) OMC-1.9N containing 15 wt % water, and (C) OMC-4.1N containing 19 wt % water. The peaks correspond with the crystallization of water within the mesopores.

For measurements of water dynamics, all of the mesoporous carbons were loaded with 10 wt% water to avoid crystallization during the QENS measurements following prior reports for partially filled mesoporous materials.[40, 41] Figure 3 illustrates the Mean Squared Displacement (MSD) as determined from the relative change in the elastic peak area on cooling for the different OMCs containing 10 wt % water. Note that without water in the pores, the MSD of the OMC-1.9N is almost negligible due to the combination of the low neutron cross-section of carbon and the solid state of the carbon framework that limits motions on the timescales resolvable by HFBS spectrometer. The relative differences in water motions can be readily ascertained from Figure 3A with the MSD decreased with increasing nitrogen content at a given temperature when T >125 K. At high temperatures, the MSD (mobility) is large and this steadily decreases on cooling. It is important to note that there is not an abrupt decrease in MSD as would be expected for crystallization of water for any of the OMCs examined. The water that is confined in the mesopores is supercooled without crystallization, consistent with DSC measurements at 10 wt % water loading. The MSD appears to collapse for all three samples at temperatures of approximately 125K and less. This collapse could be associated with the vitrification of the water in the mesopores, which would be approximately consistent with estimates of the glass transition temperature of bulk water.[42,43] The temperature dependence of the MSD is nearly fully reversible on heating back from the supercooled state (inset in Figure 3A), which indicates that the supercooling is likely not kinetically controlled.

In order to better understand the influence of the nitrogen doping on the dynamics, the MSD associated with the water confined within OMC-1.9N and OMC-4.1N is normalized by the MSD of water within the OMC-0N at the same temperature as shown in Figure 3B. Near ambient temperature, the normalized magnitude of the MSD for the doped samples is approximately 0.75 and 0.55 for OMC-1.9N and OMC-4.1N, respectively. Upon cooling, the difference in the MSD decreases, but even at 150K the mobility within the more hydrophilic pore is statistically lower than that for the water within the unmodified carbon (OMC-0N). This decrease in mobility of water as the pores becomes more hydrophilic is

consistent with some prior reports between dissimilar mesoporous materials: carbon and silica.[18, 44] This decrease in water mobility is partially attributed to strong hydration layers at the interface with the hydrophilic sample. The hydration layer is commonly estimated to be 0.5 nm thick[20], so this interfacial effect can impact a large fraction of the total absorbed water within the OMCs.

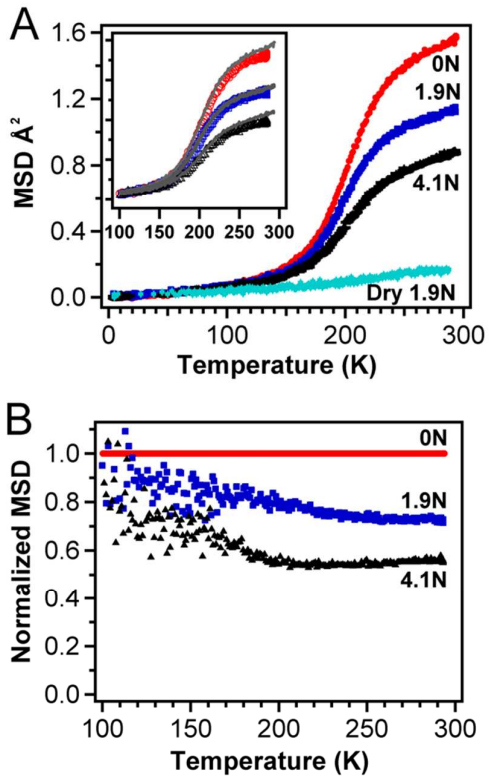


**Figure 3**. (A) MSD from QENS on cooling at 0.8K/min from room temperature to 4K for the water filled OMCs and dry (no water) OMC-1.9N. The inset in (A) shows the MSD obtained on reheating at 2K/min (open symbols) with direct comparison to the MSD on cooling (solid gray lines). (B) Normalized temperature-dependent MSD for the hydrated OMC-1.9N and OMC-4.1 relative to the OMC-0N.

More quantitative information about the mobility of water within these mesopores was obtained by fitting the quasielastic scattering with a Lorentzian model to describe the proton motions, which are directly associated with the water dynamics. Assuming that the scattering is fully elastic at 4K and the background is flat, a single Lorentzian peak can describe the broadening of the scattering due to the water dynamics. The *Q* dependence of the half width at half maximum (Γ) of the Lorentzian peak was fit to a jump diffusion model,[45] Equation 1:

$$\Gamma(Q) = \hbar D_\omega Q^2/(1 + D_\omega Q^2 \tau_o) \qquad (1)$$

where $D_\omega$ is the diffusion coefficient of water and $\tau_o$ is the time between jumps. As shown in Figure 4, Γ for most temperatures examined can be described by a jump diffusion mechanism (solid line). Based on equation 1, the linear regression of $1/\Gamma$ as a function of $1/Q^2$ also provides $D_\omega$ and $\tau_o$ from the slope and the intercept, respectively (Figure S4). As one might expect, the time between jumps increases as the temperature decreases. The effect of the chemistry of the OMC on $\tau_o$ is much weaker than the effect of temperature. As shown in Figure S5, $\tau_o$ does not appear to follow Arrhenius behaviour (scale as 1/T) for the different OMCs. The FWHM of the quasielastic peak for bulk water at temperatures as low as 260K is approximately 60 μeV, which is too fast to be resolved in the dynamic range for the instrument examined. This may account at least partially for the flat background required to fit the data at high temperatures.

As the temperature is decreased to 249K and 215K, the peak broadening decreases (Figure 4B and 4C), but the data can still be described by a jump diffusion mechanism. At the two lowest temperatures (169K and 189K), the quasielastic peak was essentially the same width as the elastic peak (at 4K). This lack of broadening at low temperatures is due to the motions of the protons becoming slower than the instrumental energy resolution. This limited change in the quasielastic peak along with the small fraction of protons within the sample contributing to this signal based on the EISF (Figure S6) challenged the accurate determination of Γ with a significant uncertainty in the fit. At 189K, Γ extracted from the optimized fit procedure[44] is noisy and cannot be described by jump diffusion as shown in Figure 4D. However, this small Γ in the OMCs is similar to reported motions of water within double (DW) carbon nanotubes (CNT) by Mamontov et al.[46] at 195 K, which are shown in Figure 4 for comparison. For these CNTs, the pore size was smaller than that of the OMCs (4.85 nm) examined here with a diameter of 1.6 nm and 1.4 nm for the double wall CNT and single wall CNT, respectively. The pure graphitic carbon matrix leads to these CNTs being more hydrophobic than the OMC, which is consistent with the increased mobility of water in more hydrophobic pores as Γ is slightly larger for the CNTs at each temperature in comparison to the OMC samples measured here. However, there is a significant difference in the pore size, which will also impact the mobility of water.

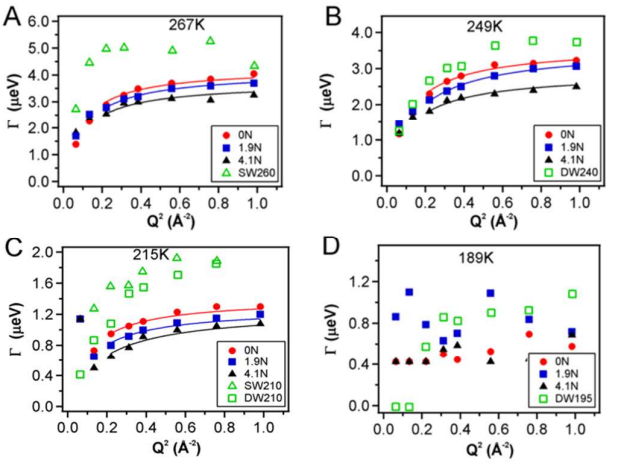


**Figure 4**. Γ obtained from Lorentzian fits of the full energy window QENS at (A) 267K, (B) 249K, (C) 215K, and (D) 189K. Γ determined from OMC samples are

shown as solid markers with the fits to jump diffusion in solid lines of the same color. These results are similar to (□) double wall (DW) and (Δ) single wall (SW) CNTs as reported by Mamontov[42] at similar temperatures.

From the fits to jump diffusion, the diffusion coefficients and activation energies of the diffusion for the water can be examined as a function of the nitrogen doping. Figure 5 shows the diffusion coefficient from the jump diffusion model at three temperatures (269K, 249K, and 215K) where the Lorentzian peak width was larger than the instrument resolution. At 290K, the proton motions of water in the OMCs are too fast to be accurately resolved with the HFBS instrument. As shown in Figure 5, water in the most hydrophobic sample, OMC-0N, exhibits the largest diffusion coefficient with decreasing diffusion coefficient with increasing nitrogen doping. The temperature dependence of the diffusion coefficient was fit with an Arrhenius equation to obtain the activation energy ($E_a$) for the self-diffusion process of the water. These results and other properties of the OMCs are listed in Table 1. The activation energy increases with increasing hydrophilicity from 158 to 209 KJ/mol from the OMC-0N to OMC-4.1N samples. This change suggests that the favorable water interaction with the N containing groups leads to a larger energy to move from the site (consistent with Figure 3 that the water confined in more hydrophilic mesopores is less mobile). This conclusion is consistent with the temperature dependence of the EISF as shown in Figure S6, indicating the changes in the wettability of the water with the pore wall impact the dynamics of water confined in mesopores of identical size.

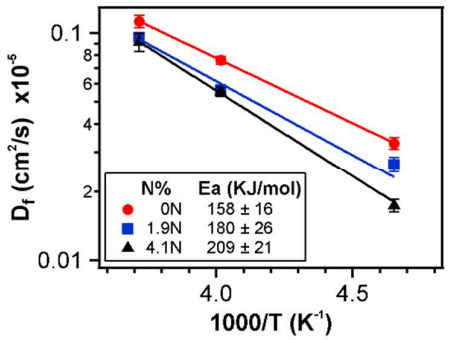


**Figure 5**. Effective diffusion coefficients of water from fits of the QENS data to a jump diffusion model with Arrhenius model fits shown as the solid lines for each data set. Error bars throughout represent one standard deviation.

**Table 1**. Pore characteristics of the OMC and different N-doped mesoporous carbons with their activation energy for the confined water self-diffusion.

| Sample | BET surface area ($m^2$/g) | Average pore size (nm) | Pore volume ($cm^3$/g) | N content (at%) | Water contact angle (º) | $E_a$ (kJ/mol) |
|---|---|---|---|---|---|---|
| OMC | 479 | 4.9 | 0.39 | 0 | 88 | 158 ± 16 |
| OMC-1.9N | 451 | 4.8 | 0.37 | 1.9 | 18 | 180 ± 26 |
| OMC-4.1N | 427 | 4.8 | 0.33 | 4.1 | ~0 | 209 ± 21 |

## Conclusions

We have demonstrated that minor doping of the carbon framework in mesoporous carbon can appreciably influence the dynamics of water confined in the mesopores when there is no change in the size of the mesopores. Nitrogen doping of the framework with 1.9 at% and 4.1 at% leads to a marked decrease in the water contact angle, but does not appreciable impact the average pore size (4.85 ± 0.05 nm). When the porous carbon contains 10 wt % water, water does not crystallize within the mesopores even on cooling at slow rates (0.8 K/min) down to 100 K irrespective of the N doping content. However, the water mobility increases with increasing hydrophobicity with the relative difference between the undoped and more doped carbon decreasing as the water supercooling increases. We attribute this difference in mobility to the absence of a highly bound hydration layer for the undoped porous carbon, which likely acts to slow water locally through hydrogen bonding with free water. This hypothesis of bound water at the interface is consistent with the dependence of the activation energy associated with water motions on the hydrophobicity of the confining material. These results provide additional insights into the role of the surface chemistry on the dynamics of water in confined environments.

## Conflicts of interest

There are no conflicts to declare.

## Acknowledgements

This work was partially financially supported by the National Science Foundation under grants no. CBET-1606685 and CBET-1159295. Access to the HFBS was provided by the center for high resolution neutron scattering, a partnership between the NIST and the National Science Foundation under Agreement No. DMR-1508249. The identification of any commercial product or trade name does not imply endorsement or recommendation by the NIST.

## References


1. H. Kiani and D.-W. Sun, *Trends Food Sci. Technol.*, 2011, **22**, 407-426.
2. N. Dalili, A. Edrisy and R. Carriveau, *Renew. Sust. Energ. Rev.*, 2009, **13**, 428-438.
3. R. Drori, C. Li, C. Hu, P. Raiteri, A. L. Rohl, M. D. Ward and B. Kahr, *J. Am. Chem. Soc.*, 2016, **138**, 13396-13401.
4. C. G. Wiener, M. Tyagi, Y. Liu, R. Weiss and B. D. Vogt, *J. Phys. Chem. B*, 2016, **120**, 5543-5552.
5. N. Pavliček and L. Gross, *Nat. Rev. Chem.*, 2017, **1**, 5-16.
6. P. Ball, *Chem. Rev.*, 2008, **108**, 74-108.
7. L. D. Gelb, K. Gubbins, R. Radhakrishnan and M. Sliwinska-Bartkowiak, *Rep. Prog. Phys.*, 1999, **62**, 1573.
8. L. Shen, Q. Che, H. Li and X. Zhang, *Adv. Funct. Mater.*, 2014, **24**, 2630-2637.
9. K. Morishige and K. Kawano, *J. Chem. Phys.*, 1999, **110**, 4867-4872.
10. K. Morishige and H. Uematsu, *J. Chem. Phys.*, 2005, **122**, 044711.
11. D. Takaiwa, I. Hatano, K. Koga and H. Tanaka, *Proc. Natl. Acad. Sci. USA*, 2008, **105**, 39-43.
12. K. Koga, G. T. Gao, H. Tanaka and X. C. Zeng, *Nature*, 2001, **412**, 802-805.
13. P. Gallo, M. Rovere and S. H. Chen, *J. Phys. Chem. Lett.*, 2010, **1**, 729-733.
14. M. Sattig and M. Vogel, *J. Phys. Chem. Lett.*, 2014, **5**, 174-178.
15. C. Yu, G. Li, X. Guan, J. Zheng, L. Li and T. Chen, *Electrochim. Acta*, 2012, **81**, 283-291.
16. E. W. Washburn, *Phys. Rev.*, 1921, **17**, 273-283.
17. X.-Q. Chu, A. Kolesnikov, A. Moravsky, V. Garcia-Sakai and S.-H. Chen, *Phys. Rev. E*, 2007, **76**, 021505.
18. A. Faraone, K.-H. Liu, C.-Y. Mou, Y. Zhang and S.-H. Chen, *J. Chem. Phys.*, 2009, **130**, 134512.
19. A. Schreiber, I. Ketelsen and G. H. Findenegg, *Phys. Chem. Chem. Phys.*, 2001, **3**, 1185-1195.
20. X. Q. Jia and T. J. McCarthy, *Langmuir*, 2003, **19**, 2449-2457.
21. I. K. Moon, S. Yoon, K. Y. Chun and J. Oh, *Adv. Funct. Mater.*, 2015, **25**, 6976-6984.
22. M. Batzill, *Surf. Sci. Rep.*, 2012, **67**, 83-115.
23. Q. Guo, D. Zhao, S. Liu, S. Chen, M. Hanif and H. Hou, *Electrochim. Acta*, 2014, **138**, 318-324.
24. Z. Qiang, Y. Xia, X. Xia and B. D. Vogt, *Chem. Mater.*, 2017, **29**, 10178-10186.
25. Z. Qiang, Y. Guo, H. Liu, S. Z. Cheng, M. Cakmak, K. A. Cavicchi and B. D. Vogt, *ACS Appl. Mater. Interfaces*, 2015, **7**, 4306-4310.
26. S. Brunauer, P. H. Emmett and E. Teller, *J. Am. Chem. Soc.*, 1938, **60**, 309-318.
27. E. P. Barrett, L. G. Joyner and P. P. Halenda, *J. Am. Chem. Soc.*, 1951, **73**, 373-380.
28. K. Morishige and S. Kittaka, *J. Phys. Chem. C*, 2015, **119**, 18287-18292.
29. K. Morishige, T. Kawai and S. Kittaka, *J. Phys. Chem. C*, 2014, **118**, 4664-4669.
30. A. Meyer, R. Dimeo, P. Gehring and D. Neumann, *Rev. Sci. Instr.*, 2003, **74**, 2759-2777.
31. Z. Qiang, Y.-M. Chen, Y. Xia, W. Liang, Y. Zhu and B. D. Vogt, *Nano Energy*, 2017, **32**, 59-66.
32. K. V. Kumar, K. Preuss, Z. X. Guo and M. M. Titirici, *The J. Phys. Chem. C*, 2016, **120**, 18167-18179.
33. L. Liu, S.-H. Chen, A. Faraone, C.-W. Yen, C.-Y. Mou, A. I. Kolesnikov, E. Mamontov and J. Leao, *J. Phys. Condens. Matter*, 2006, **18**, S2261.
34. K. Domin, K. Y. Chan, H. Yung, K. E. Gubbins, M. Jarek, A. Sterczynska and M. Sliwinska-Bartkowiak, *J. Chem. Eng. Data*, 2016, **61**, 4252-4260.
35. K. Morishige, *J. Phys. Chem. C*, 2018, **122**, 5013-5019.
36. A. Kusmin, S. Gruener, A. Henschel, O. Holderer, J. Allgaier, D. Richter and P. Huber, *J. Phys. Chem. Lett.,* 2010, **1**, 3116-3121
37. S. Gruener, D. Wallacher, S. Greulich, M. Busch and P. Huber, *Phys. Rev. E,* 2016, **93**, 013102
38 C. Sendner, D. Horinek, L. Bocque and R.R. Netz, *Langmuir*, 2009, **25**, 10768-10781.
39. L. Liu, S-H. Chen, A. Faraone, C-W. Yen, C-Y. Mou, A.I. Kolesnikov, E. Mamontov and J. Leao, *J. Phys.: Condes. Matt*, 2006, 18, S2261-S2284
40. R. Valiullin and I. Furo, *J. Chem. Phys.*, 2002, **117**, 2307-2316.
41. E. Gonzalez Solveyra, E. De La Llave, D. A. Scherlis and V. Molinero, *J. Phys. Chem. B*, 2011, **115**, 14196-14204.
42. I. Kohl, L. Bachmann, A. Hallbrucker, E. Mayer and T. Loerting, *Phys. Chem. Chem. Phys.*, 2005, **7**, 3210-3220.
43. C. A. Angell, *Chem. Rev.*, 2002, **102**, 2627-2650.
44. R. T. Azuah, L. R. Kneller, Y. Qiu, P. L. W. Tregenna-Piggott, C. M. Brown, J. R. D. Copley and R. M. Dimeo, *J. Res. Natl. Inst. Stand. Technol.*, 2009, **114**, 341-358.
45. C.T. Chudley, R.J. Elliott, *Proc. Phys. Soc.* 1961, **77**, 353-361.
46. E. Mamontov, C. Burnham, S.-H. Chen, A. Moravsky, C.-K. Loong, N. De Souza and A. Kolesnikov, *J. Chem. Phys.*, 2006, **124**, 194703.